Modeling and analysis of thin-film, piezoelectric actuators
by Ashley Erin Childs

Athesis submitted in partial fulfillment of the requirements for the degree of Master of Science . in Mechanical Engineering
Montana State University

Abstract:
This paper contains a description of the modeling and analysis of thin-film, piezoelectric actuators that were designed by a multi-discipline research team at Montana State University (MSU). The actuators consist of layers of poly(vinylidene fluoride) that are joined by epoxy and are formed into double S-curve shapes. The actuators were developed to actively control vibrations on experimental platforms in micro-gravity environments. To develop a robust active control algorithm, information about the actuator behavior was required. Analytical and finite element models were developed to provide this information, and analyses using these models were performed. The following results of the analyses are presented: the linear range of the actuator's behavior, the optimum radii of curvature, the effects of initial curvature, and the effect of the epoxy—either a uniform or non-uniform layer. This paper also shows that the analytical and finite element results correlate with each other and are reasonable when compared with experimental data. The models can therefore be used as design tools for future applications of the actuator.

MODELING AND ANALYSIS OF THIN-FILM, PIEZOELECTRIC ACTUATORS

by

Ashley Erin Childs

A thesis submitted in partial fulfillment
of the requirements for the degree

of

Master of Science

in

Mechanical Engineering

MONTANA STATE UNIVERSITY—BOZEMAN
Bozeman, Montana

January 2000

APPROVAL

of a thesis submitted by

Ashley Erin Childs

This thesis has been read by each member of the thesis committee and has been found to be satisfactory regarding content, English usage, format, citations, bibliographic style, and consistency, and is ready for submission to the College of Graduate Studies.

Dr. R. Jay Conant — (Signature) — Date 11/7/00

Approved for the Department of Mechanical Engineering

Dr. Vic Cundy — (Signature) — Date 11/7/00

Approved for the College of Graduate Studies

Dr. Bruce R. McLeod — (Signature) — Date 12-9-00

STATEMENT OF PERMISSION TO USE

In presenting this thesis in partial fulfillment of the requirements for a master's degree at Montana State University—Bozeman, I agree that the Library shall make it available to borrowers under rules of the Library.

If I have indicated my intention to copyright this thesis by including a copyright notice page, copying is allowable only for scholarly purposes, consistent with "fair use" as prescribed in the U.S. Copyright Law. Requests for permission for extended quotation from or reproduction of this thesis in whole or in parts may be granted only by the copyright holder.

Signature Ashley Elliott

Date 2/1/00

ACKNOWLEDGEMENTS

The author would like to thank NASA for financially supporting this work. The author would like to express her sincere gratitude to Dr. R. Jay Conant for his time, guidance, and advice during the development of this thesis. She would also like to thank Gary Bohannan for the helpful discussions and direction. The author is also grateful for the assistance of Erica McKenzie, Andy Ross, Michelle Galvin, Jil Hallenberg, Joe Wehri, and the entire Montana State Micro-Gravity Team.

TABLE OF CONTENTS

LIST OF TABLES

LIST OF FIGURES

LIST OF FIGURES - Continued

LIST OF SYMBOLS

CHAPTER 2

Symbol	Description
N	internal resultant normal force in a curved beam
$d\phi$	differential arc angle of a curved beam segment (cbs)
Q	internal resultant shear force in a curved beam
ds	differential arc length of a cbs
R	radius of curvature of the middle line (undeformed)
q	distributed load on a curved beam
M	internal resultant moment in a curved beam
$\vec{u}$	displacement field of a point in a cbs
$\vec{x}$	position of point P'
$\vec{X}$	position of point P
r	radius of curvature of a deformed cbs
FR	fixed reference frame
P	point in the undeformed cbs
P'	point P in the deformed cbs
$\vec{X}_o$	position of point A
A	point on the middle line of the undeformed cbs
$\vec{e}_r$	unit vector, radial direction, undeformed coordinates
y	radial distance from A to P
R'	radius to P
A'	point A in the deformed cbs

LIST OF SYMBOLS - Continued

$\vec{e}_\phi$ ..... unit vector $\perp$ to $\vec{e}_r$, undeformed coordinate system (cs)

β ..... angle between $\vec{e}_r$ and line A'P'

$\vec{x}_o$ ..... position of point A'

v ..... tangential component of the middle line displacement

w ..... radial component of the middle line displacement

u_r ..... displacement component in the radial direction

u_ϕ ..... displacement component in the tangential direction

ε_r ..... radial strain

ε_ϕ ..... tangential strain

$\gamma_{r\phi}$ ..... shear strain

h ..... thickness of the curved beam

ε_o ..... strain at the middle line

$d\phi'$ ..... differential arc angle of a cbs (deformed)

ds' ..... differential arc length of a cbs (deformed)

d_{ij} ..... piezoelectric strain coefficient: i dir. E field, j dir. strain

σ_ϕ ..... tangential stress

E_i ..... electric field intensity: i direction

Y ..... Young's modulus

b ..... width of a beam's cross-section

A ..... cross-sectional area of a beam

I ..... moment of inertia of the electroded film about the 2 axis

y_i ..... radial distance from the middle line of the i^{th} layer

Q_i ..... resultant internal shear force in the i^{th} layer

N_i ..... resultant internal normal force in the i^{th} layer

LIST OF SYMBOLS - Continued

M_i ..... resultant internal moment in the i^{th} layer

R_1 ..... radius of curvature of the middle line, inner layer (1)

R_3 ..... radius of curvature of the middle line, outer layer (3)

R ..... radius of curvature to the middle line of the bimorph

h_g ..... thickness of the epoxy layer

$\Delta\phi$ ..... small segment of a bimorph

$\varepsilon_{\phi i}$ ..... tangential strain in the i^{th} layer

E_{31} ..... electric field intensity in the 3 direction in layer 1

E_{33} ..... electric field intensity in the 3 direction in layer 3

Y_g ..... Young's modulus of the epoxy layer

A_g ..... cross-sectional area of the epoxy layer

I_g ..... moment of inertia of the epoxy layer about the 2 axis

$\Delta E_3 = E_{33}-E_{31}$ ..... difference in the electrical field intensities, layers 3 and 1

w_i ..... radial displacement of the middle line of the i^{th} layer

v_i ..... tangential displacement of the middle line of the i^{th} layer

ϕ_i ..... arc angle of the small bimorph segment for the i^{th} layer

I_{eq} ..... equivalent moment of inertia of bimorph about the 2 axis

h_{eq} ..... equivalent thickness of the bmorph

$E_3 = E_{33}+E_{31}$ ..... sum of the electrical field intensities in layers 3 and 1

ε_{oi} ..... strain at the middle line of the i^{th} layer

A_{eq} ..... equivalent cross-sectional area of the bimorph

CHAPTER 3

Symbol ..... Description

d_{ij} ..... piezoelectric strain coefficient: i dir. E field, j dir. strain

LIST OF SYMBOLS - Continued

S_{ij} ..... elastic compliance matrix components

V ..... wave speed

Δt ..... time between reflections

h ..... sample thickness

V_T ..... transverse wave speed

V_L ..... longitudinal wave speed

ν ..... Poisson's ratio

G ..... shear modulus

Y ..... Young's modulus

ρ_{avg} ..... mass density averaged over several samples

$U_x^{(R)}$ ..... reflected wave field

AR ..... magnitude of $U_x^{(R)}$

ρ^i ..... mass density of medium i

V_L^i ..... longitudinal wave speed in medium i

I ..... magnitude of the incident wave

G_g ..... shear modulus of the epoxy

Y_g ..... Young's modulus of the epoxy

CHAPTER 4

Symbol ..... Description

∂V ..... differential of the voltage

ΔV ..... voltage gradient

r_e ..... distance between electrical charges

LIST OF SYMBOLS - Continued

P ..... poling direction

L ..... length of the piezoelectric film used

ϕ_o ..... arc angle of each beam segment

ϕ_i ..... arc angle along beam segment i

β_i ..... angle that the middle line of beam segment i rotates

v_i ..... tangential displacement of beam segment i

w_i ..... radial displacement of beam segment i

Q_i ..... resultant internal shear force in beam segment i

N_i ..... resultant internal normal force in beam segment i

M_i ..... resultant internal moment in beam segment i

Δ ..... total vertical displacement of an actuator

δ ..... vertical displacement of a bimorph

R_i ..... radius of curvature of beam segment i

N_{oi} ..... reaction in the tangential direction in beam segment i

Q_{oi} ..... reaction in the radial direction in beam segment i

M_{oi} ..... reaction moment in beam segment i

M^* ..... magnitude of the constant moment

Λ_i ..... electrical terms for beam segment i

Γ_i ..... electrical term for beam segment i

A_i ..... constant, differential equation solution, beam segment i

B_i ..... constant, differential equation solution, beam segment i

C_i ..... constant, differential equation solution, beam segment i

α_i ..... particular solution for beam segment i

M_i^* ..... magnitude of the constant moment in beam segment i

LIST OF SYMBOLS – Continued

s_i ..... arc length along beam segment i

L_i ..... arc length of beam segment i at ϕ_o

E_{3i} ..... E_3, beam segment i

ΔE_{3i} ..... ΔE_3, beam segment i

$l = L / 2$ ..... length of the quarter model

$r = R_2 / R_1$ ..... ratio of the radii of curvature of the beam segments

M_A ..... externally applied moment at A

F ..... externally applied force at A

A ..... point on the middle line, free end, cantilevered beam

B ..... point on the middle line, inflection point of the beam

ϕ_o ..... arc angle of each beam segment

ϕ ..... arc angle along beam segment

R_i ..... radius of curvature of beam segment i

Q_i ..... resultant internal shear force in beam segment i

N_i ..... resultant internal normal force in beam segment i

M_i ..... resultant internal moment in beam segment i

M_o ..... moment at the inflection point, left-hand segment, 1

M_{vi} ..... piezoelectric pseudo-moment in beam segment i

M_{totali} ..... total moment in the beam segment i

C ..... point on the middle line, slightly before the fixed end

U_i ..... total strain energy in beam segment i

U_{total} ..... total strain energy in both beam segments

θ_A ..... total slope at A

δ_A ..... total vertical displacement at A

$K = F / \delta_A$ ..... stiffness of the bimorph

LIST OF SYMBOLS - Continued

K_g ..... stiffness of the bimorph with an epoxy layer

dV ..... applied voltage gradient

K_{vi} ..... slope of the voltage-displacement curves

K_{vp} ..... % difference, K_{vi} for bimorph w/ and w/out epoxy

CHAPTER 5

Symbol ..... Description

u ..... displacement field approximating polynomial

$\{T\}$ ..... mechanical stress matrix

$[c^E]$ ..... stiffness matrix at constant E field

$\{S\}$ ..... mechanical strain matrix

$[e^S]$ ..... piezoelectric matrix at constant strain

$\{E\}$ ..... electrical field matrix

$\{D\}$ ..... electrical displacement matrix

$[\varepsilon^S]$ ..... dielectric matrix at constant strain

$[s^E]$ ..... compliance matrix at constant E field

$[d^T]$ ..... piezoelectric matrix at constant stress

$[\varepsilon^T]$ ..... dielectric matrix at constant stress

ε_{ij} ..... strain components

s_{ij} ..... compliance matrix components

T_{ij} ..... stress matrix components

d_{ij} ..... piezoelectric matrix components

LIST OF SYMBOLS - Continued

E_i ..... electric field intensities

σ_{ij} ..... stress components

Y_i ..... Young's moduli in the i^{th} material direction

G_i ..... shear moduli in the i^{th} material direction

ν_{ij} ..... Poisson's ratios

ABSTRACT

This paper contains a description of the modeling and analysis of thin-film, piezoelectric actuators that were designed by a multi-discipline research team at Montana State University (MSU). The actuators consist of layers of poly(vinylidene fluoride) that are joined by epoxy and are formed into double S-curve shapes. The actuators were developed to actively control vibrations on experimental platforms in micro-gravity environments. To develop a robust active control algorithm, information about the actuator behavior was required. Analytical and finite element models were developed to provide this information, and analyses using these models were performed. The following results of the analyses are presented: the linear range of the actuator's behavior, the optimum radii of curvature, the effects of initial curvature, and the effect of the epoxy—either a uniform or non-uniform layer. This paper also shows that the analytical and finite element results correlate with each other and are reasonable when compared with experimental data. The models can therefore be used as design tools for future applications of the actuator.

CHAPTER 1

INTRODUCTION

A multi-discipline research team at Montana State University (MSU) has developed a vibration isolation system designed for use in micro-gravity environments that exist on space vehicles. The system operates using a piezoelectric actuator designed at MSU. The actuator consists of thin, piezoelectric-polymer films formed into a double S-curve shape.

The research team also developed an active control algorithm for the system. To make the algorithm more robust and to optimize the system's performance, the researchers needed to answer several questions. What were the optimum radii of curvature for the actuator? Should the radii be the same or should they be some ratio of each other? Should there be any initial curvature? Answers to these questions lay in analytical models. The analytical model could also describe the epoxy layer that joins the thin films, and it could provide valuable information about the epoxy layer's effect on actuator behavior.

The analytical models, limited due to their complexity, could not provide all the answers. A finite element model, however, could describe other effects that the analytical model could not. It could illustrate the effects of non-uniformity in the epoxy layer thickness, and perhaps more importantly, the finite element model could also answer questions about the linearity of the actuator response. Determining the linear range of the actuator's force-deflection curve was important for developing a robust control algorithm.

Finite element and analytical models were developed to eliminate unknowns about the current actuator design, but the team can also use these models in the future as design tools. They can use these design guides to create actuators for different force-deflection responses and customize them for specific applications. This paper describes the development of these models. It answers questions regarding the current actuator design, and describes how to use the tools for

future applications. The paper begins with a brief history of piezoelectricity, provides some background information, and then it develops the theory behind the analytical models. Next, the paper describes the finite element model, and finally, it discusses the results.

In the 1880's, Pierre and Jacques Curie applied pressure to a quartz crystal and discovered an electric charge was produced. Conversely, when the Curies applied an electric field to the crystal, it changed shape. They named this effect "piezoelectricity," derived from the Greek verb "piezen," to press. They determined that the piezoelectric effect is a characteristic of crystals lacking a center of symmetry [1]. This characteristic causes charges to displace asymmetrically under mechanical stress. Asymmetrically distributed charges induce dipole moments in crystals. The dipole moment causes the material surfaces to develop an effective charge. On the other hand, under the presence of an electrical field, repulsion or attraction forces displace the charges, producing mechanical strain.

Scientists failed to realize the benefits of piezoelectricity until more than 40 years later, during World War I, when Langevin used quartz to generate and receive sound waves under water. This work led to the development of sonar. Other applications followed this, such as microphones and telephone receivers [1]. Further research revealed piezoelectric behavior in many biological substances, such as proteins, cellulose, and items containing collagen. Examples of these organic substances include wool, silk, DNA, RNA, bone, tendon, muscle, and skin [1, 2].

In 1969, Kawai discovered the effect in other organic materials [3]. He found that elongated, polarized films of synthetic polymers were piezoelectric. Poly(vinylidene fluoride) (PVDF) showed the largest effect. PVDF is inherently polar because the fluorine ions are negatively charged and the hydrogen ions positively charged, and lie on opposite sides of the carbon backbone. Despite its polar molecular structure, the average dipole moment in an amorphous region of PVDF is zero due to the random orientation of the molecules along the polymer chain. However, PVDF is semi-crystalline, and it has tiny crystals embedded in the amorphous matrix. Elongating films of PVDF transforms the crystals into the polar "beta" phase.

Poling[1] orients the dipole moments of all the crystals in the same direction to produce a macroscopic polarization. Poly(vinyl chloride) (PVC) and nylon also exhibit piezoelectric properties, but the effects are not as significant as that found in PVDF.

Today piezoelectric polymers and ceramics are used in a broad range of applications: biomedical devices, ink-jet printers, structures, traffic systems, robotics, aerodynamics, vibration control, and recreational equipment [4, 5, 6, 7, 8 and 9]. In any given system, the piezoelectric material can be used as a sensor and/or an actuator. The material acts as a sensor if pressure is applied to produce a signal sent to a control system. For example, piezoelectric cables can be placed on road surfaces [5]. When a car drives over them and applies pressure, the piezoelectric material experiences a change in electric field. This produces a signal that is then transmitted to a control system, telling it a car is present. Conversely, a piezoelectric material acting as an actuator deforms if a voltage is applied. An example of piezoelectric actuators is found in some ink-jet printers [8, 9]. A miniature piston made of piezoelectric ceramic expands when a voltage is applied, reducing the volume of the ink chamber and forcing ink out of a tiny hole.

Piezoelectric ceramics are useful as actuators, but since PVDF is a compliant polymer, it is not as useful for actuator applications, especially at low frequencies [2]. Several researchers have created certain configurations of PVDF, however, which do work well as actuators for some applications. These actuators involve layers of thin films that form either straight or curved elements. Ervin and Brei [10] indicate that stacks of straight, thin film actuators can be configured to customize force-deflection behavior or frequency response. These actuators are straight elements that are joined at their ends by a spacer, illustrated in Figure 1 (modified from [10]). Each half of the actuator, L, consists of two segments of equal length, $L/2$, to which opposing piezoelectric pseudo-moments are applied.

[1] Poling is a manufacturing process. The material is heated to near or above its Curie temperature. A large voltage is then applied, which aligns the dipoles, while the material is cooled back down to ambient temperature. The dipoles are then "locked" into the new position.

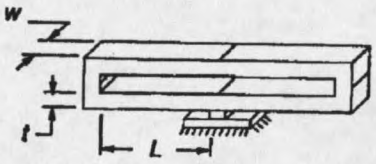

Figure 1. Straight actuator.

This design incorporates two layers of PVDF film joined by a layer of epoxy, called a bimorph. If more than two layers of PVDF film are used to create each layer of thickness "t," then the group of layers is referred to as a multi-morph.

Typically a bimorph is used in bending mode. In Figure 2 (modified from [4]), one bimorph in bending mode and one in extension mode are illustrated. To create a bimorph that operates in bending mode, the polarity (denoted P on each layer) of the material must be in opposite directions with the same electric field applied across each layer, as is shown in the figure, part A. Bending modes also exist if the polarity of the layers is in the same direction but with the electric field in each layer equal and in opposite directions. In either case, one layer will try to contract and the other layer will extend, creating the bending motion.

In the extension mode, both layers either contract or extend together. To create a bimorph that operates in this mode, the polarity of the material must be in the same direction, as is shown in Figure 2, part B. Extension mode also exists if the material polarity of each layer is opposite the other, as long as the electric field applied is equal and opposite across each layer. Figure 2 shows the cases where the electric field is equal and in the same direction in both part A and B.

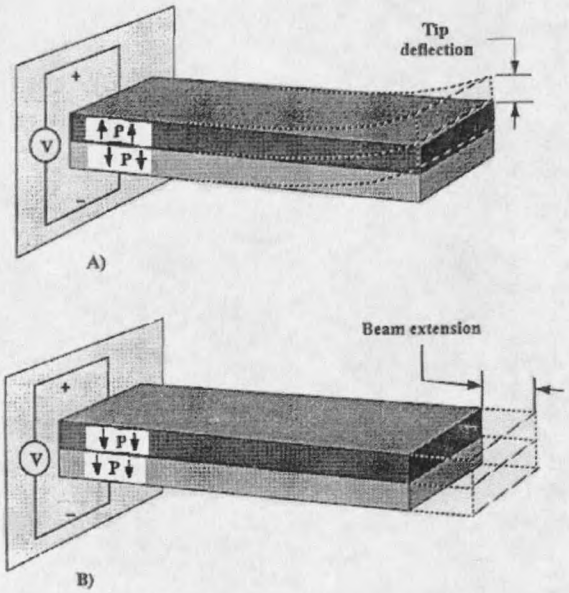

Figure 2. A) Bending mode. B) Extension mode.

Stampleman and von Flotow [12] have proposed an actuator design using the bending mode of a single circular arc, shown in Figure 3. This actuator consists of a bi- or multi-morph. The researchers specifically designed it for use in isolating vibrations in micro-gravity. Multiple actuators would be placed around an experimental platform and controlled appropriately to isolate the experiment from unwanted accelerations.

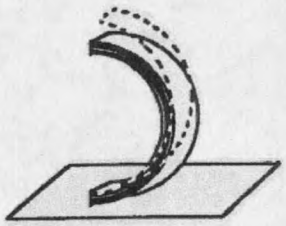

Figure 3. Single Circular Arc Actuator.

The MSU research team also developed their actuator design for vibration isolation in micro-gravity environments, like that on the space shuttle in orbit, or on the international space station. The future space station will introduce an opportunity for scientists to perform more

experiments in zero gravity, studies that might otherwise be difficult to perform on the earth due to gravity's effects. Examples of such research include the following: producing defect-free crystals, phase transitions, and combustion. Without the effects of gravity, scientists could learn more about the fundamental behavior of gases and find ways to produce more efficient combustion processes that are so critical to human life here on Earth.

Neither the space station nor the space shuttle provides a true zero-gravity environment. Such experiments would require a vibration isolation system to eliminate unwanted accelerations. These unwanted accelerations stem from both natural and man-made sources. Man-made sources include pumps operating, exercise equipment, thrusters, and closing hatches. Bodies in low-earth orbit also experience orbital disturbances. These disturbances arise when the center of gravity of the payload is not at the same altitude as that of the platform supporting it. The payload then orbits the earth at a different speed and angular rate than the platform, creating restraining forces in the supports [12].

MSU's current actuator design, shown in Figure 4 [13], consists of two bimorphs joined at their ends with no spacer between them. Note that the thicknesses of the layers are exaggerated for clarity. Each bimorph has initial curvature in a double S-shape with the inflection point at quarter length. The radius of curvature of each quarter of the bimorph is 31 millimeters. The bimorphs operate in bending mode to create an extension or contraction of the curved structure.

The bimorphs used in the current design are two inches square, made of two sheets of 28 μm PVDF film joined together by a layer of 30-minute epoxy. Silk-screened silver electrodes coat the 28-μm film, making the total thickness of the layer 45 μm. A complete bimorph has a total average thickness of 115 μm, so in the current design, the epoxy layer is 25 μm thick.

Stampleman and von Flotow suggest, through an undisclosed manufacturing process, that they are able to achieve an epoxy layer thickness of 2 μm [12]. They point out that the epoxy layers produce a stiffening effect, and they indicate that minimizing the thickness of this layer is beneficial for maximizing actuator deflection. In an effort to minimize the epoxy layer thickness in